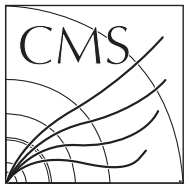

The Compact Muon Solenoid Experiment

Analysis Note

The content of this note is intended for CMS internal use and distribution only

September 10, 2009

Plans to Search for New Particles Decaying to Dijets in pp Collisions at $\sqrt{s} = 10$ TeV

Sertac Ozturk
University of Cukurova, Adana, Turkey
Visitor at Fermilab, Batavia, IL, USA

Chiyoung Jeong and Sung-Won Lee
Texas Tech University, Lubbock, TX, USA

Robert M. Harris and Konstantinos Kousouris
Fermilab, Batavia, IL, USA

Abstract

We use a simulated pseudo-data sample corresponding to $10\ pb^{-1}$ of integrated luminosity from the CMS experiment at a pp collision energy of 10 TeV to test our plans to search for new particles decaying to dijets. We describe the planned search analysis and include some early estimates of systematic uncertainties. By construction the measured dijet mass spectrum in this test agrees with the QCD prediction. Applying our search to this pseudo-data sample, we show that CMS could exclude at 95% confidence level models containing the following particles: axigluon and flavor universal coloron with mass below $1.8\ TeV$, excited quarks with mass below $1.8\ TeV$ and E_6 diquark with mass below $1.0\ TeV$ and mass between $1.3\ TeV$ and $1.7\ TeV$.

1 Introduction

In this note we document our plans and techniques to search for dijet resonances in early CMS data. The note is also intended as documentation for an early CMS paper on a first measurement of the dijet mass distribution and a dijet resonance search, for which there exists a draft version based on a simulation pseudo-data sample [1].

1.1 Models

The Standard Model (SM) is the current theory of quarks and leptons and their electromagnetic, weak, and strong interactions. However, it is not a complete theory because it has important unanswered questions, such as: Why do quarks come in different flavors? Why are the quarks arranged in generations? Why are there four different forces? How do we unify gravitation with the other forces? Why is gravity so weak? There are new theories that try to address these questions. As these theories try to answer these questions, they often predict extremely short-lived particles called resonances.

We will search for processes producing narrow resonances, X, decaying to dijets as illustrated in fig. 1: $pp \rightarrow X \rightarrow$ jet + jet (inclusive). We will perform a generic search that we can apply to any model. Here we introduce some models in order of decreasing cross section at low mass, say a few words about the cross section, and explicilty list the partons involved in production and decay, as previously written [2]. Excited states of composite quarks [3] are strongly produced giving large cross sections ($qg \rightarrow q^*$). Axigluons [4] or colorons [5] from an additional color interaction are also strongly produced, but require an antiquark in the initial state ($q\bar{q} \rightarrow A$ or C) slightly reducing the cross section compared to excited quarks. Diquarks [6] from superstring inspired E_6 grand unified models are produced with electromagnetic coupling from the valence quarks of the proton ($ud \rightarrow D$). The cross section for E_6 diquarks at high mass is the largest of all the models considered, because at high parton momentum the probability of finding a quark in the proton is significantly larger than the probability of finding a gluon or antiquark. Randall Sundrum gravitons [7] from a model of large extra dimensions are produced from gluons or quark-antiquark pairs in the initial state ($q\bar{q}, gg \rightarrow G$). Heavy W bosons [8] inspired by left-right symmetric grand unified models have electroweak couplings and require antiquarks for their production($q_1\bar{q}_2 \rightarrow W'$), giving small cross sections. Heavy Z bosons [8] inspired by grand-unified models are widely anticipated by theorists, but they are electroweakly produced, and require an antiquark in the initial state($q\bar{q} \rightarrow Z'$), so their production cross section is around the lowest of the models considered. Table 1 summarizes some properties of these models.

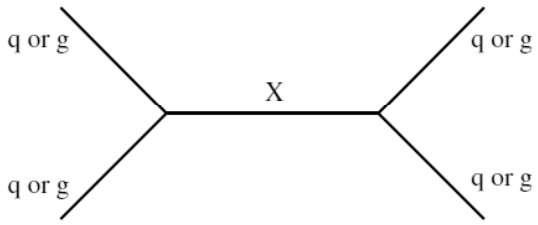

Figure 1: Feynman Diagram of dijet resonance.

Model Name	X	Color	J^P	$\Gamma/(2M)$	Chan
Excited Quark	q*	Triplet	$1/2^+$	0.02	qg
E_6 Diquark	D	Triplet	0^+	0.004	qq
Axigluon	A	Octet	1^+	0.05	$q\bar{q}$
Coloron	C	Octet	1^-	0.05	$q\bar{q}$
RS Graviton	G	Singlet	2^-	0.01	$q\bar{q}$, gg
Heavy W	W'	Singlet	1^-	0.01	$q\bar{q}$
Heavy Z	Z'	Singlet	1^-	0.01	$q\bar{q}$

Table 1: Propserties of Some Resonance Models

1.2 Summary of Experimental Technique

QCD dijet events are the dominant process in a hadron collision. Our experimental method to search for dijet resonances utilizes the dijet mass spectrum. If a resonance exists, it should appear in the dijet mass spectrum as a bump. The dijet resonance shape for generic di-parton resonances containing qq, qg and gg partons were

simulated [9] using PYTHIA [10] as resonance signals. Then, we produced a pseudo-data sample for our search. A toy generator was written to produce random statistical fluctuation in a smooth QCD background curve. It gave us a pseudo-data sample that looks like real data with $10pb^{-1}$ of integrated luminosity, under the pessimistic assumption that there are no dijet resonance signals to observe in the real data, and we will only be setting limits. We used this sample for our dijet resonance search. To calculate the upper cross section limit, we perform a binned maximum likelihood method [11]. The method gives a Poisson likelihood as a function of the cross section. We convolute the statistical likelihood distribution with our Gaussian systematic uncertainty and find the 95% confidence level upper limit on the cross section. This gives cross section limits for generic narrow qq, qg and gg resonances, independent of any specific resonance model. The upper limit on the cross section is then compared with the predicted cross section for a few models to obtain mass limits on particular models.

2 Definition of Jets and Dijet Mass Spectrum

Within the standard model events with two energetic jets (dijets) are expected to arise in proton-proton collisions from parton-parton scattering. The outgoing scattered partons manifest themselves as hadronic jets.

Jets are reconstructed using the seedless infrared safe cone algorithm with cone size $R = \sqrt{(\Delta\eta)^2 + (\Delta\phi)^2} = 0.7$ [12]. Below we will discuss three types of jets: reconstructed, corrected and generated. The reconstructed jet energy, E, is defined as the scalar sum of the calorimeter tower energies inside the jet. The jet momentum, $\vec{p}$, is the corresponding vector sum: $\vec{p} = \sum E_i \hat{u}_i$ with $\hat{u}_i$ being the unit vector pointing from the origin to the energy deposition E_i inside the cone. The jet transverse momentum, p_T, is the component of $\vec{p}$ in the transverse plane. The E and $\vec{p}$ of a reconstructed jet are then corrected for the non-linear response of the calorimeter to a generated jet. Generated jets come from applying the same jet algorithm to the Lorentz vectors of stable generated particles before detector simulation. The corrections are chosen so that, on average, the p_T of a corrected jet is equal to the p_T of the corresponding generated jet. The corrections used for this simluation analysis are the CMS standard relative and absolute jet corrections for η and p_T variation of the jet response. More details on jet reconstruction and jet energy corrections can be found in [13, 14].

The dijet system is composed of the two jets with the highest p_T in an event (leading jets), and the dijet mass is given by $m = \sqrt{(E_1 + E_2)^2 - (\vec{p}_1 + \vec{p}_2)^2}$. For both leading jets required to have pseudorapidity $|\eta| < 1.3$. The sample we plan to use in the real data will be collected by requiring at least one jet in the high level trigger with $p_T > 110$ GeV/c. The trigger efficiency, which will be measured from a sample acquired with a prescaled trigger with a lower p_T threshold, should be greater than 99% for dijet mass above 420 GeV/c^2 [15]. It is possible to include jet data selected with a lower p_T threshold and prescales in the analysis as well, to gain more sensitivity for lower mass resonances, but here we have restricted ourselves to the simpler analysis that utilizes only one unprescaled trigger for the purpose of analysis speed. Backgrounds from cosmic rays, beam halo, and detector noise are expected to occasionally produce events with large or unbalanced energy depositions. They will be removed by requiring $\not\!\!E_T / \sum E_T < 0.3$ and $\sum E_T < 10$ TeV, where $\not\!\!E_T$ ($\sum E_T$) is the magnitude of the vector (scalar) sum of the transverse energies measured by all calorimeter towers in the event. This cut is more than 99% efficient for both QCD jet events and the signals of new physics considered. In the high p_T region relevant for this search, jet reconstruction is fully efficient. Then, the dijet mass spectrum is formed as follows;

$$\frac{d\sigma}{dm_{jj}} = \frac{1}{\int Ldt} \frac{N_i}{\Delta m_{jj}} \tag{1}$$

where N_i is the number of events in the i-th dijet mass bin, Δm_{jj} is the i-th dijet mass bin width.

In Fig. 2 we present our pseudo-data of the inclusive dijet mass distribution for $pp \to 2jets + X$, where X can be anything including additional jets.We plot the differential cross section versus dijet mass in bins approximately equal to the dijet mass resolution. The black curve is a smooth QCD curve from PYTHIA+CMS simulation. The data points are produced around this smooth QCD curve with statistical fluctuation. The data points are one pseudo-data sample: one possible experimental outcome arising from a parent sample equal to the black curve. The band shows the systematic uncertainties we expect on the data and the dashed curve shows the next-to-leading order QCD calculation [15]. The purpose of this figure in a real publication of a null search result would be as a confidence builder that the data is in reasonable agreement with QCD within uncertainties, and there is no significant evidence for dijet resonances. The plot is not meant as a detailed test of perturbative QCD or as a means of reporting the differential cross section to the community.

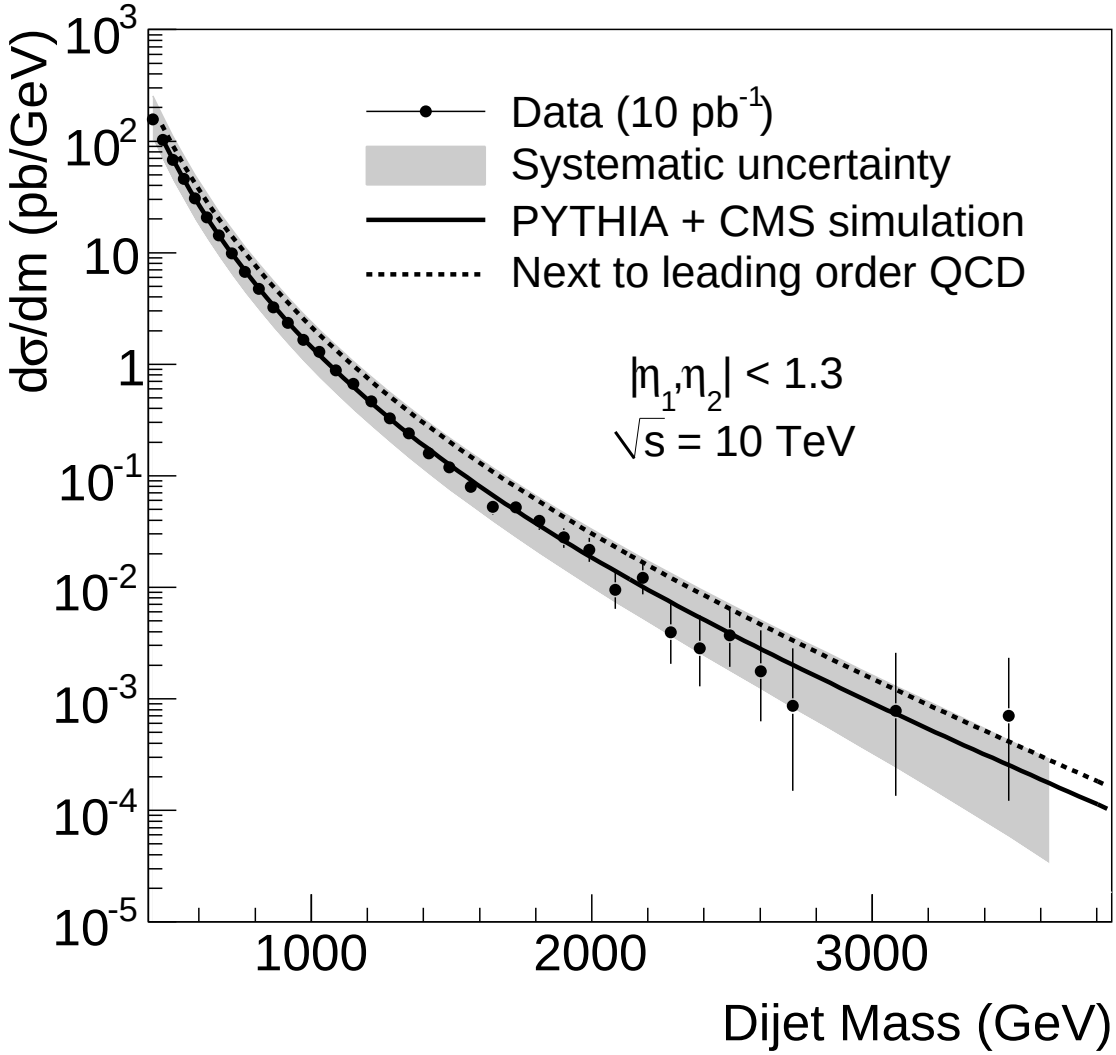

Figure 2: The dijet mass distribution from our pseudo-data sample (points) compared to a simulation of QCD and the CMS detector (solid curve) and a next-to-leading order QCD calculation (dashed curve). The band shows the systematic uncertainty on the data arising primarily from the jet energy scale.

2.1 The Signal: Dijet Resonances

The process of $q* \rightarrow qg$, $G \rightarrow q\bar{q}$ and $G \rightarrow gg$ were produced using PYTHIA [10]+CMS simulation at three different masses of $0.7\ TeV$, $2\ TeV$ and $5\ TeV$ [9]. The Fig. 3 shows the dijet mass distribution of excited quarks for GenJets, CaloJets and Corrected CaloJets at three different resonance masses. The peaks of GenJets and Corrected CaloJets are roughly at the expected resonance mass. The low mass tail in the resonance shape comes predominantly from FSR (Final State Radiation) and the high mass tail is enhanced by ISR (Initial State Radiation). [9]

Dijet mass resolution as a function of resonance mass is illustrated in Fig. 4. The resolution is calculated as $Sigma/Mean$ which is obtained from Gaussian fit to the core of the dijet mass distribution. It is well fit by function of

$$\frac{\sigma}{Mean} = 0.042 + \frac{31.7}{M_{Res}} \tag{2}$$

where M_{Res} is resonance mass. The resolution varies from 10% at $0.7\ TeV$ to 5% at $5\ TeV$ and is consistent with

previous studies [19].
In Fig. 5, we present the resonance shapes which come from the process of $q* \rightarrow qg$, $G \rightarrow q\bar{q}$ and $G \rightarrow gg$ at three different masses of $0.7\ TeV$, $2\ TeV$ and $5\ TeV$. Because of different detector response, ISR and FSR, the resonance shapes are different. The width of dijet resonances increases with number of gluon because gluons emit more radiation than quarks. These and further details of the resonance shape are discussed in a separate note [9].

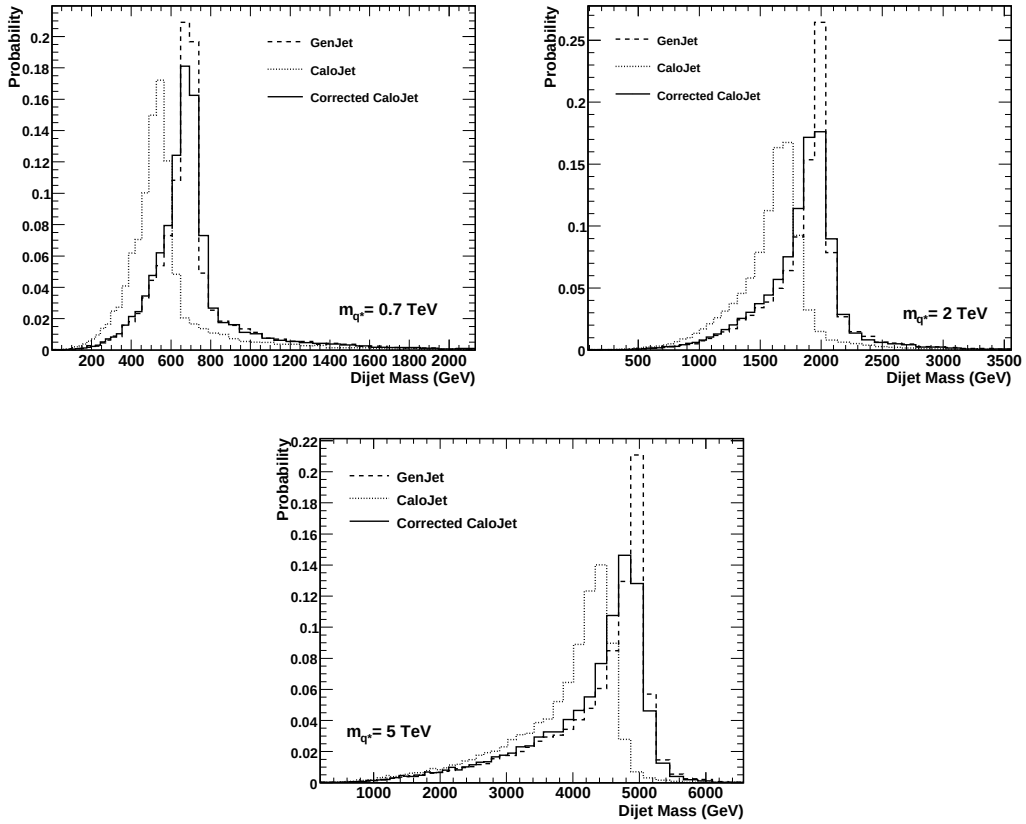

Figure 3: Dijet mass distribution for excited quark of mass at $0.7\ TeV$ (left plots), $2\ TeV$ (middle plots), and $5\ TeV$ (right plots), for GenJets, CaloJets and Corrected CaloJets.

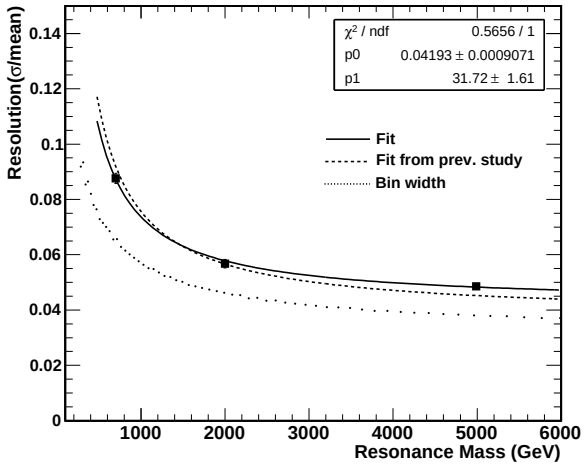

Figure 4: The dijet mass resolution as a function of resonance mass.

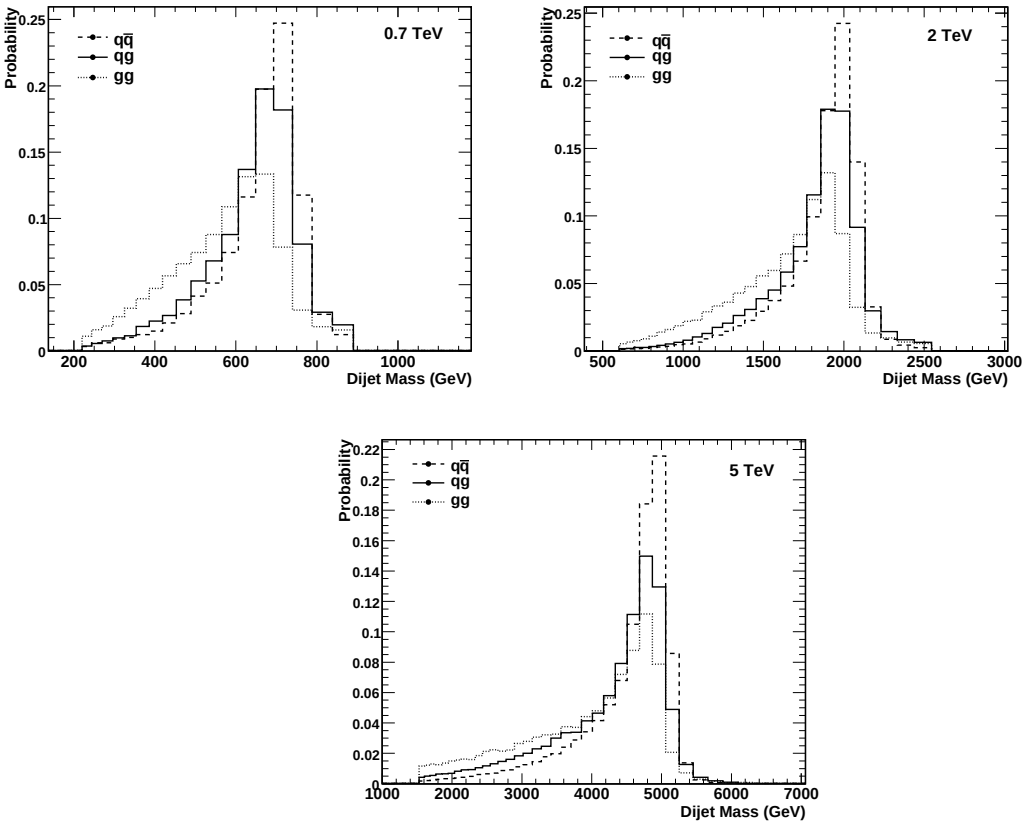

Figure 5: Dijet mass distribution for $q\bar{q}$ (qq), qg and gg resonances of mass at $0.7\,TeV$ (left plots), $2\,TeV$ (middle plots), and $5\,TeV$ (right plots).

The resonance shape at resonance mass values between the generated values are obtained using an interpolation technique. First, we defined a new parameter as $x = \frac{M_{jj}}{M_{Res}}$ where M_{jj} is dijet mass and M_{Res} is resonance mass. Then we generated the X distribution of any resonance mass between generated Monte Carlo resonance masses. Finally for resonances of mass M between generated samples for resonances of mass $M1$ and $M2$, we apply the equation

$$Prob_M(x) = Prob_{M1}(x) + \Big[Prob_{M2}(x) - Prob_{M1}(x)\Big] \cdot \frac{M - M1}{M2 - M1} \tag{3}$$

For example, If we want to generate the X distribution of resonances with a mass at $1TeV$, we use the equation below. Since $1\,TeV$ is between $0.7\,TeV$ and $2\,TeV$, we used the MC sample masses at $0.7\,TeV$ and $2\,TeV$. It gives the probability in each X bins of mass at $1TeV$.

$$Prob_{1TeV}(x) = Prob_{0.7TeV}(x) + \Big[Prob_{2TeV}(x) - Prob_{0.7TeV}(x)\Big] \cdot \frac{1 - 0.7}{2 - 0.7} \tag{4}$$

Finally, the X distribution was converted to variable dijet mass bins using interpolation technique to get resonance shape at any resonance masses. Fig. 6 shows the X distribution at $0.7\,TeV$, $2\,TeV$ and $5\,TeV$ from MC samples on the left side. The comparison of X distribution between $0.7\,TeV$, $1\,TeV$ and $2\,TeV$ is illustrated on the right side. The X distribution at $1\,TeV$ is between $0.7\,TeV$ and $2\,TeV$ as expected.
Fig. 7 shows the resonance shape of excited quark. The resonance shapes with solid lines come directly from generated Monte Carlo (MC) samples. The dashed lines show the resonance shape which come from the interpolation technique for excited quarks of mass at $1\,TeV$, $3\,TeV$ and $4\,TeV$. It can be seen clearly that the interpolation technique yields reasonable intermediate shapes, and we have verified that the interpolation technique gives exactly the generated shapes at the endpoints. We use these resonance shapes to calculate cross section upper limit at any resonance mass.

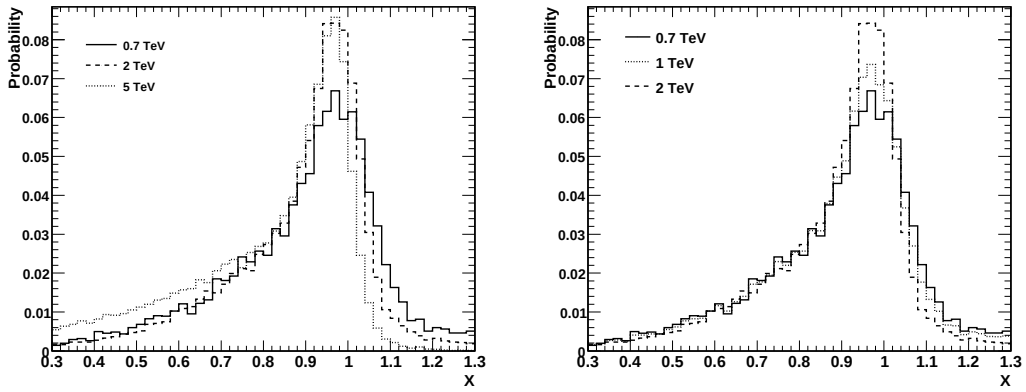

Figure 6: X distribution for excited quark of mass at $0.7\,TeV$, $2\,TeV$ and $5TeV$ (left plot). X distribution of mass at $1\,TeV$ compared with mass at $0.7\,TeV$ and $2\,TeV$ (right plot).

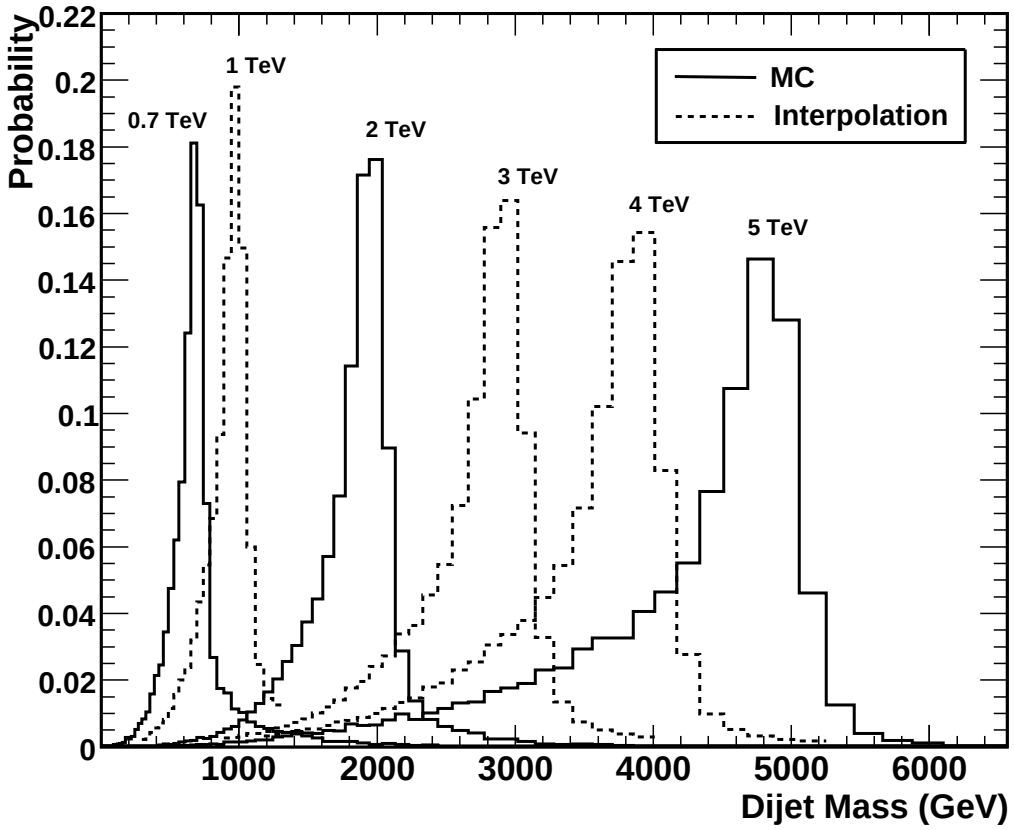

Figure 7: Resonance shapes at various resonance masses using interpolation technique compared with MC samples.

2.2 The Background: QCD Dijet

All QCD dijet events are considered background. Inclusive dijet production $(pp \to 2jets + X)$ is the dominant pp process, predicted by QCD scattering of partons. After cleanup of backgrounds from cosmic rays, beam halo and detector noise using the $\not\!\!E_T / \sum E_T < 0.3$ requirement, QCD dijet events are the only significant background for the dijet resonance search. We generated a pseudo-data set with statistical fluctuation in smooth QCD background curve which already was discussed in Section 2. Fit function with four parameters was chosen as equation 5. We get a reasonable χ^2 of 23 for 32 degrees of freedom.

$$\frac{d\sigma}{dm} = p_0 \frac{(1 - \frac{m}{\sqrt{s}} + p_3(\frac{m}{\sqrt{s}})^2)^{p_1}}{(m/\sqrt{s})^{p_2}} \tag{5}$$

In Fig. 8, we present three different plots. The top plot in Fig. 8 shows the differential cross section of excited quark signals as a function of dijet mass with background fit. The bottom left plot shows the differences between the data and the fit function in units of the statistical error. These pulls, defined as *(Data-Fit)/Error*, are consistent with statistical fluctuations and are oscillating around zero. In the bottom right plot the fractional difference between the pseudo-data and the smooth background fit is compared to resonance signals. This *(Data-Fit)/Fit* plot as a function of dijet mass shows qualitatively that q* signals with resonance mass less than roughly $2\ TeV$ could be seen or excluded. These plots demonstrate how a simple parametrization can be used to find the standard model background in a search for dijet resonances, even if there are substantial uncertainties in the direct comparison between data and a fixed QCD prediction.

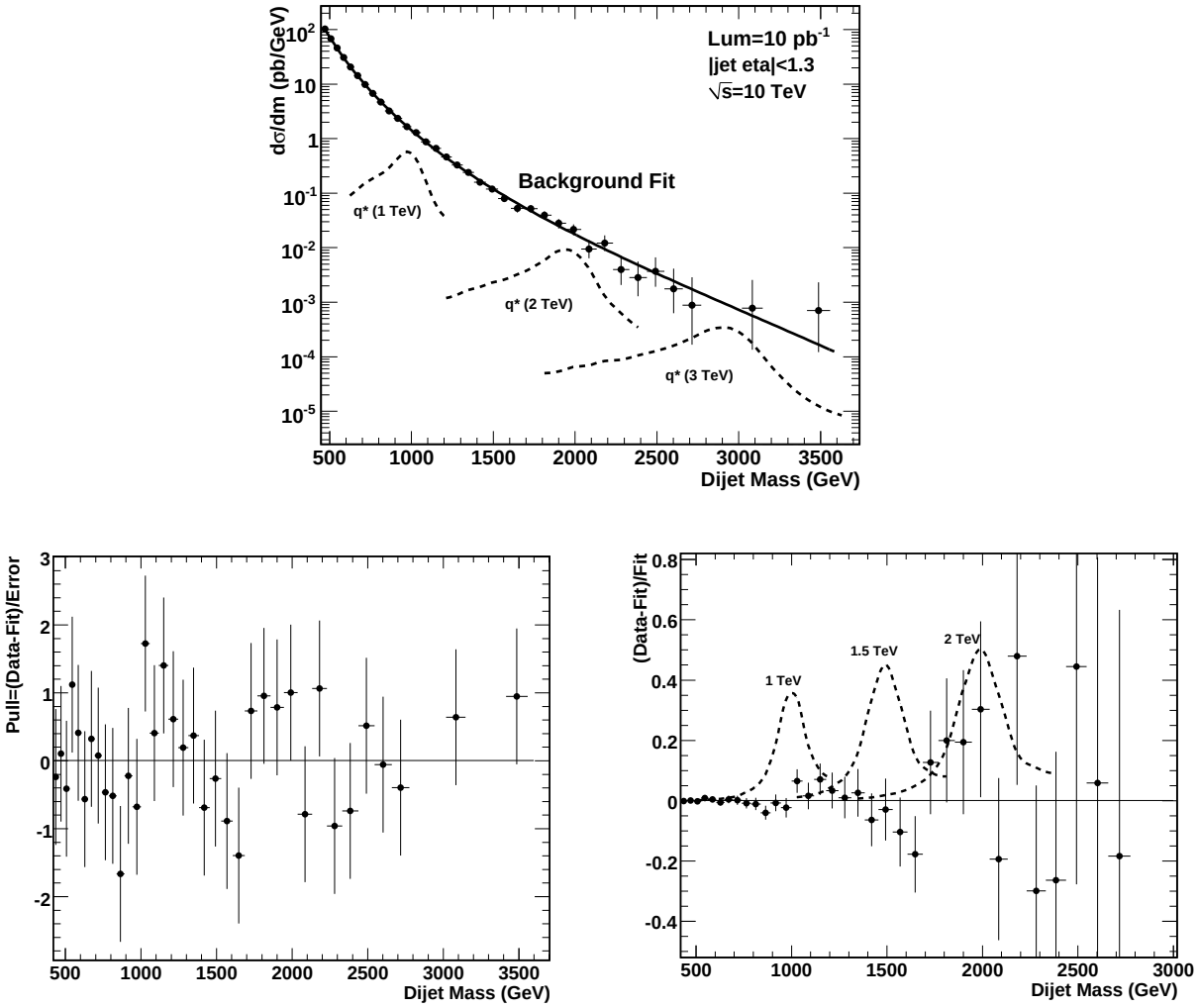

Figure 8: *The top plot*: The dijet mass distribution (points) compared to a smooth background fit (solid curve) and to a simulation of excited quarks signals in the CMS detector (dashed curves). *The bottom left plot*: (Data-Fit)/Error versus dijet mass is shown. *The bottom right plot*: The fractional difference between the dijet mass distribution (points) and a smooth background fit (solid line) is compared to simulations of excited quark signals in the CMS detector (dashed curves).

3 Search for Dijet Resonances

3.1 Likelihoods

A Bayesian technique based on a binned likelihood [11] is used to calculate the limits on new particle production. The likelihood as a function of the signal normalization, α, can be written as:

$$L = \prod_i \frac{\mu_i^{n_i} e^{-\mu_i}}{n_i!} \tag{6}$$

where

$$\mu_i = \alpha N_i(S) + N_i(B). \tag{7}$$

n_i is measured number of events in the $i-th$ dijet mass bin, $N_i(S)$ is number of events from signal in the $i-th$ dijet mass bin, α multiplies the signal and $N_i(B)$ is number of expected events from background in the $i-th$ dijet mass bin. We consider that QCD background is fixed to the best $Signal + QCD$ fit to data point and it gives the expected number of background event in the $i-th$ dijet mass bin,$N_i(B)$. This simple and conservative method takes any upward fluctuation observed in the data consistent with a resonance as an actual resonance, and finds the background beneath it from the simultaneous fit to the background parametrization plus resonance signal, as was done in an early search at the Tevatron [16]. The number of signal in the $i-th$ dijet mass bin,$N_i(S)$,comes from the interpolation technique on a signal for a qq, qg or gg resonance with arbitrary cross section. The signal multiplier α sets the expected signal rate, $N_i(S)$ is the signal shape, and the signal cross section in a bin is αN_i divided by the integrated luminosity. The signal range is chosen from $0.3 \cdot M_{Res}$ to $1.3 \cdot M_{Res}$ since low mass tail is effectively lost in QCD background and resonance shapes beyond 1.3M are highly model dependent for narrow resonances and not trusted. The signal cross section is the sum of the cross sections per bin over the signal range. We the plot the likelihood distribution as a function of the signal cross section for resonances with mass from 0.7 TeV to 3.5 TeV in 0.1 TeV steps. Examples of likelihood distributions are shown in Fig. 9 for qg resonances at six different resonance masses.

In Fig. 9 we see likelihood distributions characteristic of searching a wide mass spectrum for a resonance. The likelihood distributions at 1.5, 2.5 and 3 TeV peak at zero signal cross section, indicating that the data in that region is either below or at the background fit on average. Other likelihood distributions at 1, 2 and 3.5 TeV peak at non-zero signal cross section, with low significance, indicating that the data in that region is above the background fit on average. Taking a look back at the bottom left plot of Fig. 8 confirms that this is indeed the case, and the likelihood distributions reflect the statistical fluctuations inevitable over a wide mass spectrum. For the case of the 2 TeV resonance the fluctuation is particularly strong, roughly at the level of 2σ, and produces a significant increase in the upper limit discussed below.

We find the 95% confidence level upper limit on the cross section including only statistical uncertainties, σ_{95}, from the following

$$\frac{\int_0^{\sigma_{95}} L(\sigma)d\sigma}{\int_0^{\infty} L(\sigma)d\sigma} = 0.95 \tag{8}$$

Examples of σ_{95} values are graphically illustrated in Fig. 8.

3.2 Upper Cross Section Limit with Statistical Error

We calculated the 95% confidence level upper limit for resonances of $q\bar{q}$ (or qq), qg and gg. Fig. 10 compares the cross section limit with statistical uncertainties only to calculated resonance cross section for six different models. As discussed in the previous section, the bumps in the limit around 1 TeV and 2 TeV are caused by fluctuations with low significance in the data around the same mass ranges.

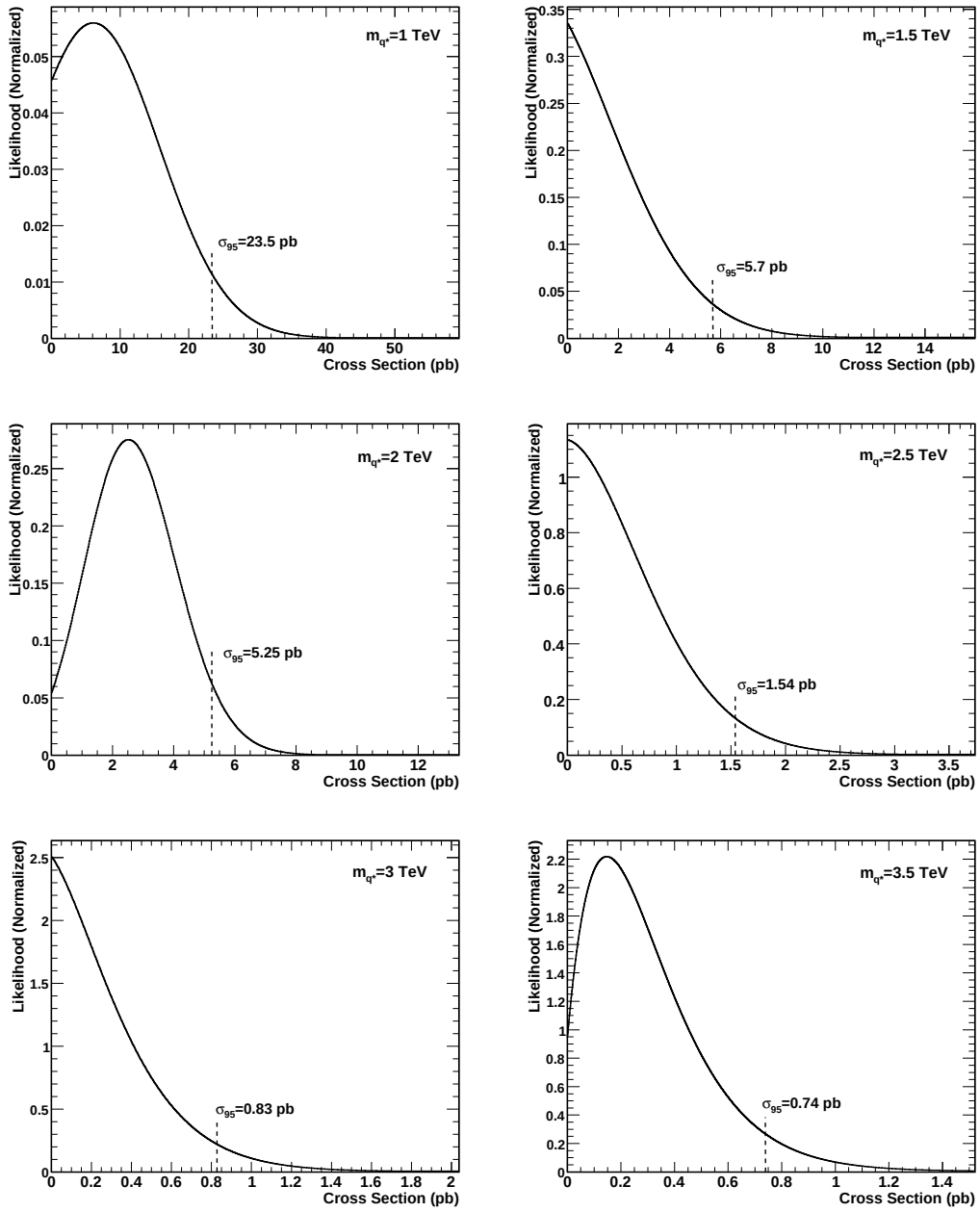

Figure 9: Likelihood distribution with 95% C.L. cross section limit at various resonance masses for excited quark resonances (Statistical error only).

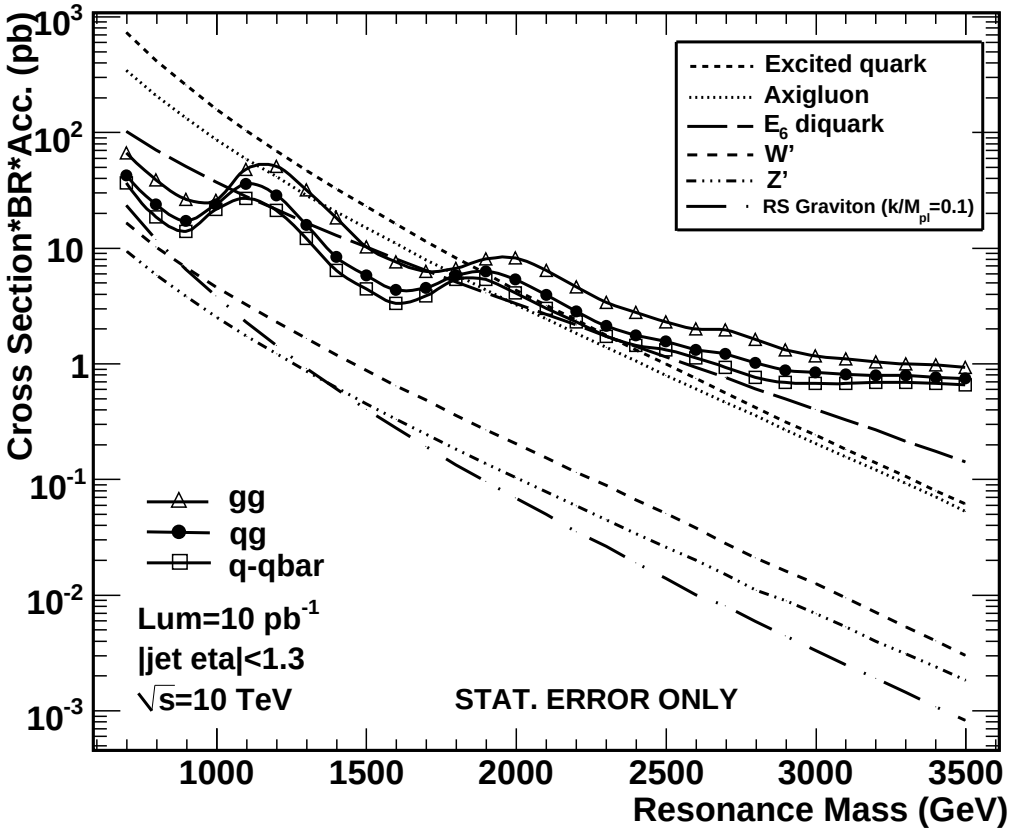

Figure 10: Dijet resonance sensitivity for 10 pb^{-1}. 95% C.L. is compared to the cross section for various resonance models. This sensitivity contains statistical error only.

3.3 Systematic Uncertainties

We have considered so far the following sources of systematic uncertainty. This is not a complete list, but it contains what we believe to be the dominant systematic uncertainties.

- Jet energy scale (JES)
- Background parametrization
- Luminosity

Jet Energy Scale (JES): The uncertainty on JES is basically the relative error between the jets in the signal simulation and where the signal would emerge in the real data. A systematic error on the jet energy scale is a systematic uncertainty on where a resonance signal of a given resonance mass would appear in the actual measured dijet mass spectrum. We assume that the uncertainty on JES is roughly $\pm 10\%$ and the signal simulation has a 1σ chance of being off by 10% in dijet mass at startup. If the signal simulation is currently 10% higher in dijet mass than the true value, and we need to shift it by 10% lower in mass, then there is really more QCD background underneath the signal than we anticipated, and finding the resonance signal is harder. The corresponding limits will be worse. However, just shifting the signal and repeating the limits suffers from statistical fluctuations in the data, producing unrealistic variations in some regions more characteristic of the exact spot the resonance is shifted to than to the actual expected uncertainty. To solve this problem we start with a smooth version of the limits: an expected limit rather than an actual limit. The left plot in Fig. 11 shows smooth cross section limit without systematics and with systematics on JES uncertainty for qg resonance. To get smooth cross section limit curve, expected events from background, $N_i(B)$, which is smooth and comes from the fit function are considered as the measured number of events, n_i, in the $i-th$ dijet mass bin. The smooth limit curve with 10% JES error then comes from shifting the signal by 10% and repeating the limits, roughly equivalent to simply shifting the smooth limit curve itself to lower mass by 10% which the reader can do by eye. Fractional change between smooth limits with and without JES uncertainty are illustrated separately for $q\bar{q}$ (or qq), qg and gg resonances in the right plot of Fig. 11. The uncertainty on JES varies roughly from 45% at $0.7\ TeV$ to 30% at $3.5\ TeV$.

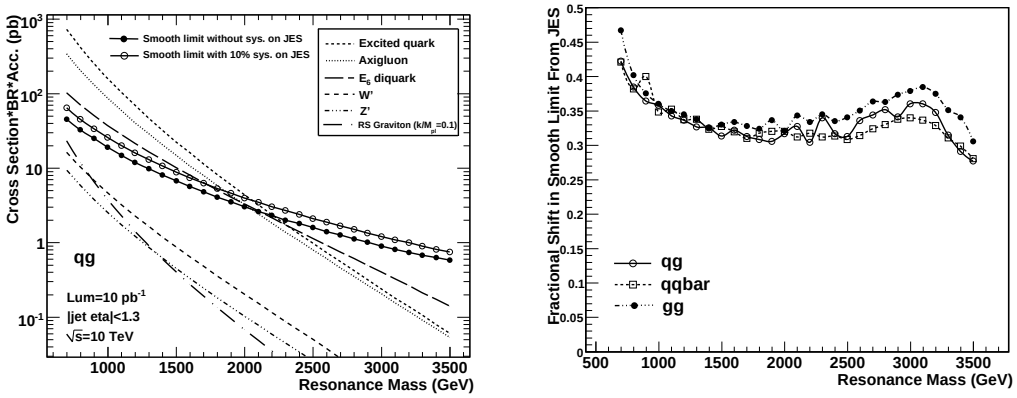

Figure 11: *Left plot*: Comparison of smoothed cross section limit without systematics and with systematic on JES uncertainty. *Right plot*:Fractional change on limit with JES systematic uncertainty.

Background Parametrization Systematic: We considered the others functional forms with 3 and 4 parameters to parametrize the QCD background. Both functional forms were used by CDF [20].

$$\frac{d\sigma}{dm} = p_0 \frac{(1-X)^{p_1}}{X^{p_2}} \tag{9}$$

$$\frac{d\sigma}{dm} = p_0 \frac{(1-X)^{p_1}}{X^{p_2+p_3 ln(X)}} \tag{10}$$

where $X = \frac{m_{jj}}{\sqrt{s}}$. Fig. 12 show comparison of fits with the data points. We found the 3 parameter form gave the largest fractional change and we used it for Background Parametrization Systematic. The right plot in Fig. 12

presents absolute fractional change on limit for qg resonances. We smoothed the statistical variations in the absolute change in the limit with a quadratic fit. The systematic uncertainty varies from 8% at $0.7\,TeV$ to 40% at $3.5\,TeV$. The same effect is observed for $q\bar{q}$ (or qq) and gg resonances.

Luminosity: We assumed an uncertainty on luminosity of about 10% at startup.

We now have the uncertainty in the limit for each source of systematic uncertainty. To find total the total systematic we add these uncertainties in quadrature. The individual and total systematic uncertainties as a function of resonance mass are illustrated in Figure 13. Absolute uncertainty in the cross section limit for each resonance mass is calculated as the total fractional systematic uncertainty multiplied by upper cross section limit.

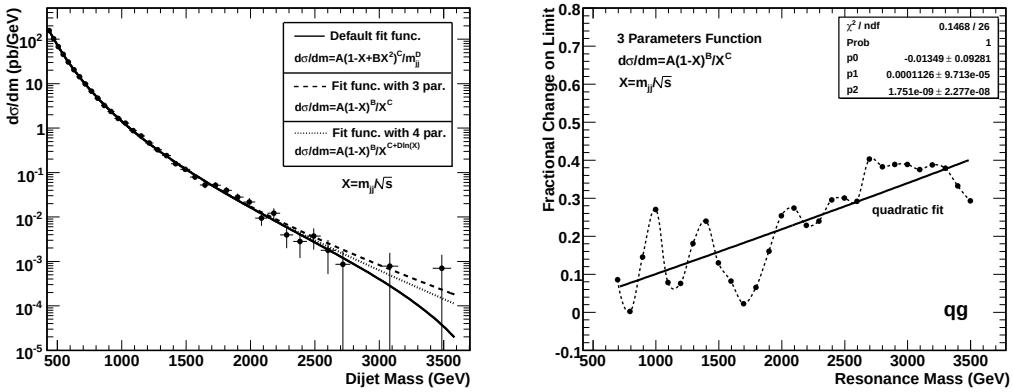

Figure 12: *Left plot*: Comparison of fit functions for background parametrization. *Right plot*:Absolute fractional change on limit with smooth quadratic fit.

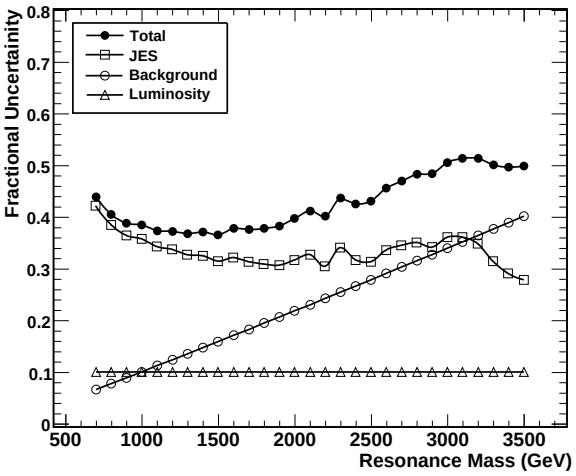

Figure 13: Fractional systematic uncertainties on signal cross section.

3.4 Upper Cross Section Limit including Systematics

We convolute the statistical likelihood distributions with our Gaussian systematic uncertainties. The width of the Gaussian is taken as the absolute uncertainty in the cross section limit for each resonance mass. The equation of convolution is [11]:

$$L(\sigma') = \int_0^\infty L(\sigma)G(\sigma)d\sigma \tag{11}$$

Likelihood distributions before and after convolution with systematic uncertainties are shown in Figure 14 along

with the 95% CL cross section values. The method we are using for considering the systematics here is oriented towards obtaining conservative limits. Probability is not allowed to shift into negative cross section values. The systematic uncertainties smear the likelihood and shift it conservatively towards higher values of signal cross section, giving larger (worse) values of the 95% CL upper limits on the cross section.

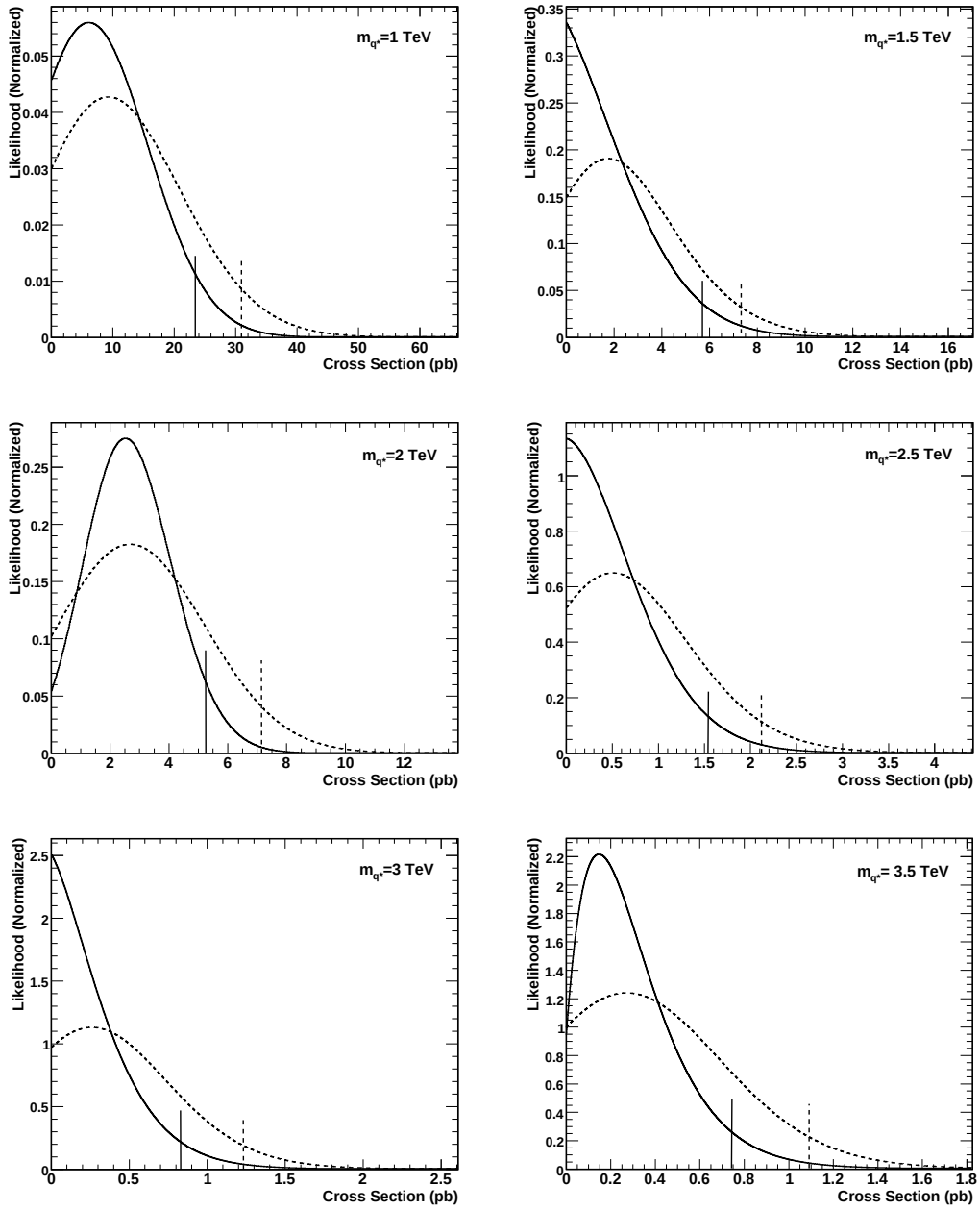

Figure 14: Likelihood distribution with 95% C.L. cross section limit at various excited quark resonance masses including systematics. Solid line is 95% C.L. cross section limit with statistical error only. Dashed line shows 95% C.L. cross section limit with including systematics.

Fig. 15 shows the cross section limit for qg resonance with and without all systematic uncertainties. Fractional change between limits for all resonances types are shown in Fig. 16. The cross section limits vary roughly from 40% at 0.7 TeV to 20% at 3.5 TeV. Fig. 15 shows that this seemingly significant change in the cross section limit produces a change in the mass limits of only about 0.1 TeV, or around 5%, because the theory curves for the cross section fall so rapidly with increasing mass. Thus systematics will not have a large effect on the mass limit for most models with large cross sections.

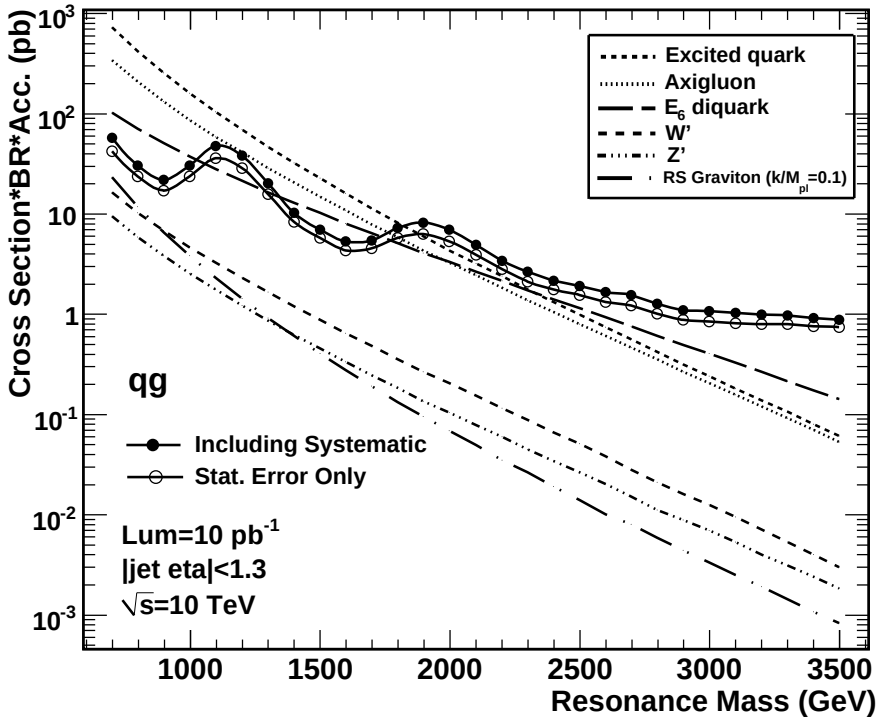

Figure 15: Cross section limits for qg resonance with and without systematic uncertainties.

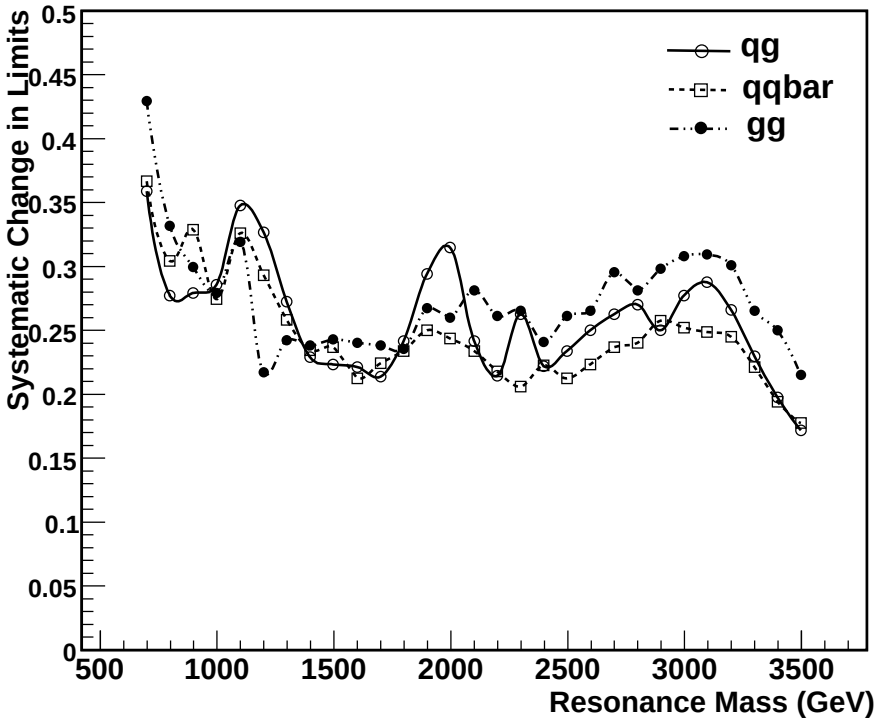

Figure 16: Fractional change on limit with including systematics.

Mass	95% C.L. $\sigma \cdot B$ (pb)		
(TeV)	qq	qg	gg
0.7	51	60	95
0.8	25	31	52
0.9	19	23	35
1.0	28	31	34
1.1	37	48	64
1.2	28	39	63
1.3	16	21	40
1.4	8.3	11	23
1.5	5.7	7.3	14
1.6	4.2	5.6	9.9
1.7	4.9	5.8	8.3
1.8	6.9	7.6	8.8
1.9	7.1	8.4	11
2.0	5.4	7.2	11
2.1	4.0	5.3	9.0
2.2	3.0	3.7	6.4
2.3	2.2	2.9	4.8
2.4	1.9	2.4	3.9
2.5	1.8	2.1	3.3
2.6	1.5	1.9	2.9
2.7	1.3	1.8	2.9
2.8	1.0	1.5	2.4
2.9	0.95	1.3	2.0
3.0	0.94	1.2	1.8
3.1	0.95	1.2	1.7
3.2	0.97	1.2	1.6
3.3	0.97	1.2	1.6
3.4	0.95	1.1	1.5
3.5	0.92	1.1	1.5

Table 2: As a function of new particle mass we list our 95% C.L. upper limit on cross section times branching ratio for narrow resonances decaying to dijets with $|\eta| < 1.3$

4 Results

The dijet resonance search results from our pseudo-data sample with 10 pb^{-1} are listed in table 2 and illustrated in Fig. 17. The 95% CL upper limits on the cross section are generic upper limits that can be compared with any model calculation for which resonances that decay to dijet with the cut $|\eta| < 1.3$ included in the cross section calculation. Presenting limits this way allows theorists to propose any new model and immediately compare their ideas with our upper cross section limits, and makes the search results have lasting value to the community. We do this comparison with a few models ourselves to serve as benchmarks and illustrate the process.

We compare the 95% CL upper limit on the cross section to the theory cross section for each model as a function of the input resonance mass. All theory predictions are lowest order calculations for dijets with $|\eta| < 1.3$ using CTEQ6L parton distributions which were described in detail previously [2]. For resonance masses where the theory curve lies above our upper limit on the cross section for the appropriate pair of partons we would exclude that model with 95% CL if the real data sample were like our pseudo-data sample. For axigluons (or colorons), which decay to $q\bar{q}$, we would use our limits on qq resonances to exclude the mass range $0.7 < M(A) < 1.8$ TeV, which would extend the previous exclusions [20] of $120 < M(A) < 1250$ GeV/c^2. For excited quarks, which decay to qg, we would use our limits on qg resonances to exclude the mass range $0.7 < M(q*) < 1.8$ TeV/c^2, which would extend the previous exclusions [20] of $260 < M(q*) < 870$ GeV/c^2. For E_6 diquarks,

which decay to qq, we would use our limits on qq resonances to exclude the mass range $0.7 < M(D) < 1.0\,TeV$, and $1.3 < M(D) < 1.7\,TeV$, which would extend the previous exclusions [20] of $290 < M(D) < 630$ GeV/c^2. The limits that arrive from this pseudo-data sample and the actual published exclusions [20] are summarized in Table. 3.

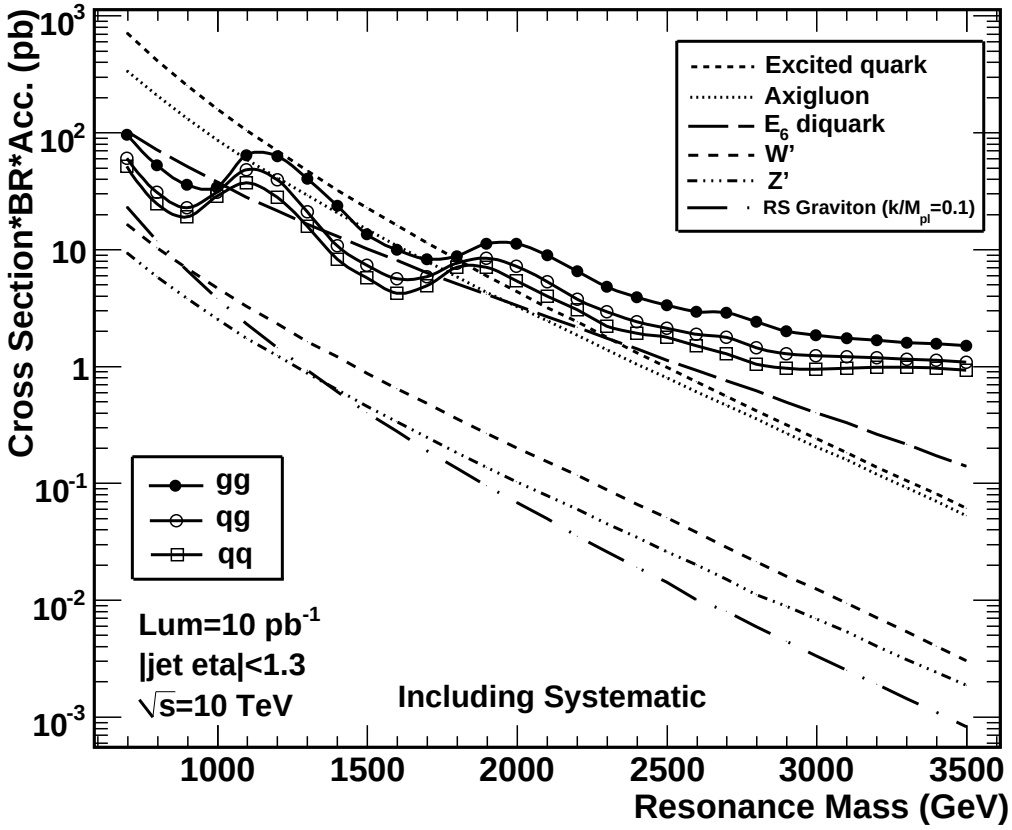

Figure 17: Pseudo-data on the 95% CL upper limit on the cross section times branching ratio for new particles decaying to dijets with partons of type gluon-gluon (solid circles), quark-gluon (open circles), and quark-quark (open boxes) are compared to theoretical predictions for various models. The limit and theory curves require that both jets have pseudorapidity $|\eta| < 1.3$.

Model Name	95% C.L. Excluded Mass (TeV)	
	CMS ($10\,pb^{-1}$, $\sqrt{s} = 10\,TeV$)	CDF ($1\,fb^{-1}$, $\sqrt{s} = 1.96\,TeV$)
Excited Quark	$M(q*) < 1.8\,TeV$	$M(q*) < 0.87\,TeV$
Axigluon, Coloron	$M(A) < 1.8\,TeV$	$M(A) < 1.25\,TeV$
E_6 Diquark	$M(D) < 1.0\,TeV$, $1.3 < M(D) < 1.7\,TeV$	$M(D) < 0.63\,TeV$

Table 3: 95% C.L. Excluded Mass for various models

5 Conclusion

We have illustrated how we plan to search for dijet resonances in the dijet mass spectrum at CMS. From a simulated pseudo-data sample arising from the QCD prediction for $10\,pb^{-1}$ of integrated luminosity at a collision energy of 10 TeV, we measure the mass spectrum, fit the background, and search separately for qq, qg, and gg resonances. If we observed this sample, which by construction did not contain any resonances, we would set upper limits on the cross section for generic dijet resonances which can be compared with the cross section for any theoretical model which decays to dijets with $|\eta| < 1.3$. If we observed this sample, we would exclude at 95% confidence level models containing the following particles: axigluon and flavor universal coloron with mass below $1.8\,TeV$, excited quarks with mass below $1.8\,TeV$ and E_6 diquark with mass below $1.0\,TeV$ and mass between $1.3\,TeV$

and $1.7\ TeV$. This would significantly extend the existing limits from the Tevatron.

References

[1] Sertac Ozturk, Chiyoung Jeong, Kostas Kousouris, Robert Harris and Sung-Won Lee, "Measurement of the Dijet Mass Distribution and Search for New Particles in pp Collisions at 10 TeV", QCD-09-006, (2009).

[2] K. Gumus et al., "CMS Sensitivity to Dijet Resonances", CMS Note 2006/070.

[3] U.Baur, I.Hinchliffe and D.Zeppenfeld, Int.J.Mod.Phys.A2 (1987) 1285.

[4] P. Frampton and S. Glashow, Phys. Lett. B190(1987)157.

[5] E.H.Simmons, Phys. Rev. D55 (1997) 1678.

[6] J.L.Hewett and T.G.Rizzo, Phys.Rept.183 (1989) 193.

[7] L.Randall and R.Sundrum, Phys.Rev.Lett.83 (1999) 4690.

[8] E.Eichten, I.Hinchliffe, K.D.Lane and C.Quigg, Rev.Mod.Phys.56 (1984) 579.

[9] Chiyoung Jeong et al., "Dijet Resonance Shapes for $\sqrt{s} = 10$ TeV", CMS AN-2009/145 (2009).

[10] T. Sjostrand, L. Lonnblad, S. Mrenna, hep-ph/0108264.

[11] J.Conway, CDF Pub.Note (2005) 6428

[12] G. P. Salam and G. Soyez, JHEP 0705:086 (2007).

[13] CMS Collaboration, CMS Physics Analysis Summary JME-07-002 (2008). at http://cms-physics.web.cern.ch/cms-physics/public/JME-07-002-pas.pdf .

[14] CMS Collaboration, CMS Physics Analysis Summary JME-07-003 (2008). at http://cms-physics.web.cern.ch/cms-physics/public/JME-07-003-pas.pdf .

[15] Kostas Kousouris et al., "Measurement of the Dijet Mass Cross Section in pp Collisions at 10 TeV", QCD-09-005 (2009).

[16] F. Abe et al., CDF Collaboration, "Search for New Particles Decaying to Dijets at CDF", Phys.Rev.D55:5263-5268,1997.

[17] R. Adolphi et al., CMS Collaboration, JINST 3:S08004 (2008).

[18] CMS Collaboration, Physics TDR Volume I, CERN-LHCC-2006-001.

[19] M.Cardaci et al.,CMS AN-2007/039, (2007)

[20] T.Aaltonen et al., CDF Collaboration, "Search for new particles decaying into dijets in proton-antiproton collisions a $\sqrt{s} = 1.96$ TeV", Phys.Rev.D78:012008 (2008)